

Collective excitations in chiral Stoner magnets

Zhiyu Dong, Olumakinde Ogunnaike, and Leonid Levitov¹

¹*Department of Physics, Massachusetts Institute of Technology, Cambridge, MA 02139*

We argue that spin and valley-polarized metallic phases recently observed in graphene bilayers and trilayers support chiral edge modes that allow spin waves to propagate ballistically along system boundaries without backscattering. The chiral edge behavior originates from the interplay between the momentum-space Berry curvature in Dirac bands and the geometric phase of a spin texture in position space. The edge modes are weakly confined to the edge, featuring dispersion which is robust and insensitive to the detailed profile of magnetization at the edge. This unique character of edge modes reduces their overlap with edge disorder and enhances the mode lifetime. The mode propagation direction reverses upon reversing valley polarization, an effect that provides a clear testable signature of geometric interactions in isospin-polarized Dirac bands.

Stoner ferromagnetism is a correlated electron order ubiquitous in topological materials of current interest, including moiré graphene[1–6], and nontwisted graphene bilayers and trilayers [7–11]. Yet, the fundamental properties of this state, especially those governed by Berry curvature in k space, are presently poorly understood. Here we predict that this state hosts chiral spin excitations. These excitations are confined to system edges and domain boundaries between different valley-polarized regions, propagating along them in a manner resembling Quantum Hall (QH) edge states, as illustrated in Fig.1. The microscopic origin of this behavior is the geometric phase of carrier spins tracking magnetization along carrier trajectories. Carrier spin rotation by a position-dependent magnetization generates a Berry phase in direct space that serves as a spin-dependent magnetic vector potential that couples to the orbital dynamics of carriers (see Eqs.(4),(5)) [12–15]. The chiral edge behavior arises due to the coupling between this geometric magnetic field and orbital magnetization due to Berry curvature in k space. The geometric character of this interaction ensures robust chiral edge physics even in “vanilla” spin-polarized Fermi seas such as those seen in Refs.[7–11].

The band magnetism of carriers exhibiting orbital magnetization is a broad framework applicable to a diverse range of systems. This includes, in particular, the QH ferromagnets [16–19] and correlated excitonic phases in QH bilayers [20–24]. Orbital magnetization in these systems exists due to Landau levels rather than the k -space Berry curvature and in QH bilayers the layer index plays the role of spin in our analysis. Here we focus on chiral edges in spin-polarized metals and, afterwards, comment on possible extensions to the QH systems.

In graphene multilayers [7–11], the predicted chiral edge behavior is sensitive to valley polarization. In a valley- and spin-polarized phase (identified as a quarter metal in Refs.[7–11]), the band orbital magnetization exhibits opposite signs in valleys K and K' . As a result, the chirality (i.e., the propagation direction) of edge modes flips upon reversing the valley imbalance.

A very different behavior is expected in a valley-

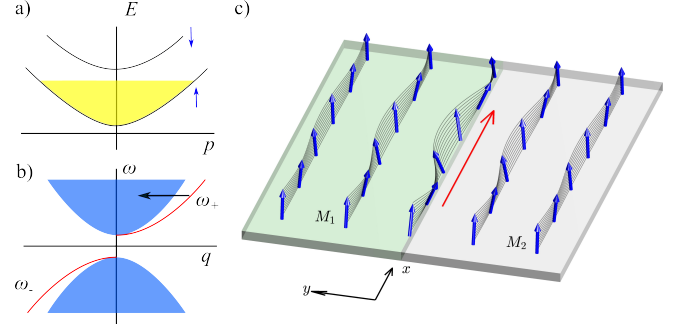


FIG. 1. (a) Schematic band structure of a fully spin-polarized Stoner phase in a valley-polarized graphene bilayer or trilayer. Only the valley populated by carriers is shown. (b) The spin-wave edge mode dispersion obtained for a step in orbital magnetization $M_1 \neq M_2$ induced by a gate, Eq.(12). The mode (red) is positioned outside the bulk magnon continuum (blue). The group velocity $v_g = d\omega/dq$ of a constant sign indicates the chiral character of the mode. The edge-to-bulk scattering (black arrow) is blocked by the energy and momentum conservation. (c) Schematic of the spatial dependence of the edge mode. The chiral mode is confined to the step and propagates along it without backscattering.

unpolarized but spin-polarized phase (half-metal in the nomenclature of Refs.[7–11]). In this case, the two valleys host Stoner metals with the band orbital magnetization of opposite signs. In this phase, the edges will host pairs of counter-propagating chiral edge modes, one for each valley. These two modes together respect the orbital time reversal symmetry, unbroken in the half-metal phase, i.e. the system is non-chiral.

The exceptional cleanness of graphene multilayers makes them an appealing system to probe this behavior. Spin lifetimes as long as 6 ns measured in large bilayer graphene (BLG) systems by a nonlocal Hanle effect at 20 K [25] are explained by residual magnetic disorder [26, 27]. In contrast, recently, it was demonstrated that electrons isolated from edge disorder by gate confinement and trapped in gate-defined quantum dots acquire ultra-long spin lifetimes, reaching values of 200 μ s [28] and 50 ms [29] when measured in an applied magnetic field by

pulsed-gate spectroscopy. Therefore, probing spin excitations in gate-defined electron puddles presents a distinct advantage. Yet, spin lifetimes measured in large BLG systems [25] also lie in a suitable range. Spin lifetimes can be further increased by applying nonquantizing magnetic fields that, apart from a constant offset, have little impact on the chiral spin-wave dispersion (see Eq.(18)).

In a metallic state the chiral mode at the edge can, in principle, decay by scattering into the 2D spin-one particle-hole continuum and spin waves. The former process is blocked by energy conservation since the spin-one continuum is gapped at small momenta [see Fig. 2 (a)]. The latter process, as shown by the black arrow in Fig.1 (b), is blocked by the energy and momentum conservation for a smooth edge but can be viable for a rough edge. However, as discussed in [30], in the long-wavelength limit the edge modes have vanishing overlaps with the edge disorder potential, a property that protects the modes from edge-to-bulk scattering.

The chiral edge behavior in a Stoner metal phase discussed here is distinct from that predicted for magnetic phases with a nontrivial magnon band topology [31–37]. In these systems, chiral edge excitations lie above the first magnon band and are therefore gapped. To the contrary, the chiral modes described here arise at the boundary of a uniformly spin-polarized Stoner Fermi sea—a metallic compressible state with a nontopological bulk magnon band. The edge excitations are gapless (in the absence of an externally applied magnetic field, see below) and have dispersion positioned beneath that of bulk spin waves (in our case these are nothing but the gapless magnons of a Heisenberg ferromagnet). Accordingly, here chiral modes arise in the absence of microscopic spin-dependent interactions such as Dzyaloshinskii-Moriya interaction (DMI) or dipolar interaction (as in Refs.[31–35] and Refs.[36, 37], respectively). Instead, they originate from an interplay between the exchange interaction and orbital magnetization in bands with Berry curvature and broken time reversal symmetry. Our spin waves act analogously to the chiral edge plasmons predicted for such bands [38], yet they transport spin rather than charge and arise from a very different mechanism.

Collective spin dynamics, both bulk and edge, are readily analyzed in the long-wavelength limit, at frequencies below the Stoner continuum [see Fig. 2 (a)]:

$$\Delta = Un_s > \omega(q), \quad (1)$$

where Δ is the Stoner gap, U is the exchange interaction, n_s is spin-polarized carrier density and $\omega(q)$ is mode dispersion. We employ an effective action for spin variables obtained by integrating out fermion orbital degrees of freedom. In that, we assume the electron velocity is large compared to that of spin-waves, $v_F \gg v_g = d\omega/dk$. As found below, the long-wavelength spin-wave dispersion is quadratic, $\omega(k) \sim k^2$, a behavior that confirms the separation of time scales for the orbital and spin degrees of

freedom and justifies our analysis. The effective action for spin variables takes the form [see e.g. [39, 40]]

$$A = \int dt d^2r (in_s S_0 \langle \eta(\mathbf{r}, t) | \partial_t | \eta(\mathbf{r}, t) \rangle - \mathcal{H}[\mathbf{n}]), \quad (2)$$

where the first term is the Wess-Zumino-Witten action, hereafter referred to as A_{WZW} , representing the single-spin Berry phase accumulated through time evolution. The second term is the Hamiltonian of a spin-polarized state discussed below. The quantity $|\eta(\mathbf{r}, t)\rangle$ represents a coherent spin state in (2+1)D space-time. Here $n_s = n_\uparrow - n_\downarrow$ is the density of spin-imbalanced carriers, the factor $n_s S_0$ is the spin density, where $S_0 = \hbar/2$. In what follows spin polarization is described by a unit vector

$$\mathbf{n}(\mathbf{r}, t) = \langle \eta(\mathbf{r}, t) | \boldsymbol{\sigma} | \eta(\mathbf{r}, t) \rangle.$$

The term $\mathcal{H}[\mathbf{n}]$ in Eq.(2) is the effective spin Hamiltonian. Symmetry arguments and microscopic analysis predict [41] the long-wavelength Hamiltonian

$$\mathcal{H}[\mathbf{n}] = n_s \left[\frac{J}{2} (\partial_\mu \mathbf{n})^2 - M(r) B(\mathbf{r}, t) - \mathbf{h}_0 \cdot \mathbf{n} \right]. \quad (3)$$

Here J is spin stiffness, the second term is an interaction between the band orbital magnetization and the geometric magnetic field, the last term is the Zeeman energy per carrier, with the g -factor and Bohr magneton absorbed in the external magnetic field \mathbf{h}_0 .

As indicated above, the interaction $-MB$ originates from a geometric Berry phase, arising due to electron spins tracking magnetization along electron trajectories. Spin rotation generates a Berry phase in position space defined by a spin-dependent magnetic vector potential [12]

$$a_\mu = \frac{\hbar c}{2e} (1 - \cos \theta) \partial_\mu \phi, \quad \mu = x, y. \quad (4)$$

Here θ and ϕ are the polar and azimuthal angles measured with respect to the spin polarization axis in the ground state. The sign of a_μ is chosen to describe the Berry phase accrued by the majority-spin carriers. For the minority-spin carriers the vector potential is of the opposite sign and is described by $-a_\mu$, giving a Berry phase of the opposite sign. The geometric magnetic field is simply the curl of a_μ . In terms of \mathbf{n} , it reads:

$$B(\mathbf{r}, t) = \nabla \times \mathbf{a} = \frac{\phi_0}{4\pi} \mathbf{n} \cdot (\partial_x \mathbf{n} \times \partial_y \mathbf{n}), \quad (5)$$

where $\phi_0 = hc/e$ is the flux quantum. This physics was first discussed in the early literature on high T_c superconductivity [42–45] and later in the literature on noncollinear magnetic systems [12–15]. Importantly, unlike static spin textures in the latter systems, our spin-wave dynamics generate a time-dependent vector potential, Eq.(4). This yields a geometric electric field [14, 46]

$$E_\mu = -\partial a_\mu / c \partial t - \nabla a_0 = \frac{\hbar}{2e} \mathbf{n} \cdot (\partial_t \mathbf{n} \times \partial_\mu \mathbf{n}), \quad (6)$$

which can enable electrical detection of the spin waves.

The quantity $M(r)$ in the second term in Eq.(3) describes the orbital magnetization per carrier in a spin-imbalanced band arising due to Berry curvature in k space. It is given by a sum of contributions of the filled states in the spin-valley-polarized Fermi sea. For a partially spin-polarized Fermi sea the contributions to M from the majority-spin and minority-spin carriers are of opposite signs, giving $M = M_\uparrow - M_\downarrow$. The opposite signs originate from the opposite signs of a_μ for the spin-up and spin-down carriers discussed beneath Eq.(4). These opposite sign contributions cancel in a spin-unpolarized state but lead to $M \neq 0$ in a fully or partially spin-polarized state. The position dependence $M(r)$ reflects spatially varying spin or valley imbalance arising, e.g., due to gating.

The geometric fields a_μ , B and \mathbf{E}_μ are derived in the adiabatic regime when an electron spin tracks spin texture along the electron's trajectory. The adiabatic regime occurs when the spin texture is sufficiently long-wavelength such that the Stoner spin gap $\Delta = Un_s$ is much greater than $\hbar v_F q$, where q is the characteristic spin-wave wavenumber and U is the exchange interaction (see Eq.(1)).

The Hamiltonian, Eq.(3), features different phases depending on the M and J values [41]. If $M > 2J$ and h_0 is small enough, the uniformly polarized state is predicted to become unstable towards twisting, giving rise to a skyrmion texture with a nonzero chiral density B . Here, we consider excitations in a uniformly polarized state

$$\mathbf{n}(r, t) = \mathbf{n}_0 + \delta\mathbf{n}(r, t), \quad \delta\mathbf{n} \perp \mathbf{n}_0, \quad (7)$$

with $\mathbf{n}_0 \parallel \mathbf{h}_0$, occurring for not too large M values.

The spin wave dispersion can be obtained from the canonical equations of motion found from the saddle-point condition $\delta A / \delta \mathbf{n} = 0$, with A given in Eq.(2). Indeed, the variation of the Wess-Zumino-Witten term A_{WZW} [the first term in Eq.(2)] can be found by noting that this term equals to $n_s S_0$ times the solid angle swept by \mathbf{n} . As a result, its variation can be expressed as

$$\delta A_{\text{WZW}} = n_s S_0 \int dt d^2 r (\delta\mathbf{n} \times \partial_t \mathbf{n}) \cdot \mathbf{n}, \quad (8)$$

The variation of the action in Eq.(2) gives $\delta A = (n_s S_0 \partial_t \mathbf{n} \times \mathbf{n} - \delta \mathcal{H} / \delta \mathbf{n}) \cdot \delta \mathbf{n}$, giving equations of motion:

$$n_s S_0 \partial_t \mathbf{n}(r) = \mathbf{h}(r) \times \mathbf{n}(r), \quad \mathbf{h} = -\frac{\partial \mathcal{H}}{\partial \mathbf{n}} + \partial_\mu \frac{\partial \mathcal{H}}{\partial \partial_\mu \mathbf{n}}. \quad (9)$$

Linearizing about a uniformly polarized state yields coupled linear equations for $\delta\mathbf{n}$ components, which are identical to those found for a nonchiral problem,

$$S_0 \partial_t \delta\mathbf{n}(r, t) = \mathbf{h}_0 \times \delta\mathbf{n}(r, t) + J \partial_\mu^2 \delta\mathbf{n}(r, t) \times \mathbf{n}_0. \quad (10)$$

Plane wave solutions to this equation yield a simple isotropic and non-chiral spin-wave dispersion

$$\omega_\pm(q) = \pm(h_0 + Jq^2)/S_0, \quad (11)$$

with values approaching $\pm h_0/S_0$ in the limit $q \rightarrow 0$, universally and independent of the exchange interaction, as required by the Larmor theorem.

For a spatially uniform M , the $-MB$ term is a topological invariant. Therefore, a local twist of spin does not change the \mathcal{H} value. As a result, this interaction neither affects the energy nor impacts the spin waves. A spatially varying M , to the contrary, has a profound effect on spin waves. In particular, system boundaries and interfaces between regions in which M takes different values support chiral spin-wave modes reminiscent of the QH edge states. To illustrate this behavior we consider a step

$$M(y) = \begin{cases} M_1, & y > 0 \\ M_2, & y < 0. \end{cases} \quad (12)$$

In this case, after linearization, Eq.(7), we find

$$\mathbf{h} = n_s [J \partial_\mu^2 \delta\mathbf{n} - \partial_y M(y) (\mathbf{n}_0 \times \partial_x \delta\mathbf{n}) + \mathbf{h}_0]. \quad (13)$$

Other terms vanish at first order in $\delta\mathbf{n}$. As a result, the linearized equations of motion become

$$S_0 \partial_t \delta\mathbf{n} = \mathbf{h}_0 \times \delta\mathbf{n} + J \partial_\mu^2 \delta\mathbf{n} \times \mathbf{n}_0 + m \delta(y) (\mathbf{n}_0 \times \partial_x \delta\mathbf{n}) \times \mathbf{n}_0,$$

where $m = M_2 - M_1$ is the difference between M on two sides of the edge. These equations are solved by writing $\delta\mathbf{n}(x, y)$ as a superposition of complex-valued helical components:

$$\delta\mathbf{n}(r, t) = \begin{pmatrix} \delta n_x(r, t) \\ \delta n_y(r, t) \end{pmatrix} = \sum_q e^{iqx} \left[e^{-i\omega_+ t} \psi_{q,+}(y) \begin{pmatrix} 1 \\ i \end{pmatrix} + e^{-i\omega_- t} \psi_{q,-}(y) \begin{pmatrix} 1 \\ -i \end{pmatrix} \right], \quad (14)$$

where we carried out the Fourier transform in time and the translation-invariant x direction. Plugging this ansatz into the equations of motion for $\delta\mathbf{n}(r, t)$, we obtain two decoupled 1D problems for a quantum particle in a delta-function potential, separately for each helicity:

$$S_0 \omega_\pm \psi(y) = \pm [h_0 + J(q^2 - \partial_y^2)] \psi - m q \delta(y) \psi(y), \quad (15)$$

where $\psi(y)$ is a shorthand for $\psi_{q,\pm}(y)$. These equations support bound states which are edge spin waves for the helical polarization of a plus (minus) sign for mq of a positive (negative) sign, respectively.

Indeed, the bound state is described by an exponential solution for both helicities:

$$\psi_{q,\pm}(y) = u_q e^{-\lambda_q |y|}, \quad \lambda_q > 0, \quad (16)$$

where the condition $\lambda_q > 0$ is required for the mode to be normalizable. The value of λ_q and the dispersion are determined by the condition

$$0 = \pm 2J\lambda_q\delta(y) - mq\delta(y), \quad (17)$$

which gives $\lambda_q = \pm \frac{mq}{2J}$. Therefore, the right-helicity mode ψ_+^q exists only for $mq > 0$, whereas the left-helicity mode ψ_-^q exists only for $mq < 0$.

$$\omega_{\pm}(q) = \pm \frac{1}{S_0} \left[h_0 + \left(J - \frac{m^2}{4J} \right) q^2 \right] \quad (18)$$

The resulting dispersion is illustrated in Fig.1 (b) for $m > 0$. The group velocity $v_g = d\omega/dq$ is of the same sign for both helicities, as expected for a chiral edge mode. At $q = 0$, the frequency value agrees with the Zeeman frequency for a single spin, as required by Larmor's theorem. At this point λ_q vanishes, which signals that the mode ceases to be confined to the edge and transforms into a uniformly precessing state.

Notably, the discrete chiral mode, Eq.(18), appears in a robust manner regardless of magnetization values in the two halfplanes and the step size $m = M_1 - M_2$. At M_1 approaching M_2 the chiral mode, while remaining discrete, approaches the bulk magnon continuum and merges with it at $M_1 = M_2$. Another interesting aspect of the dispersion in Eq.(18) is that the group velocity reverses when m exceeds $2J$, upon which the mode propagation direction is reversed, with the left-moving excitations becoming right-moving and vice versa. In this regime the frequencies $\omega_{\pm}(q)$ reverse their signs when the wavenumber reaches a certain critical value, $q = q_* = \sqrt{4Jh_0/(4J^2 - m^2)}$. Frequency sign reversal signals an instability towards a spatial modulation at the edge with spatial periodicity $2\pi/q_*$. Notably, this instability can occur before skyrmions are nucleated in the bulk. This happens, in particular, when M_1 and M_2 are of opposite signs. In this case, the condition for skyrmion nucleation in the bulk, $2J < |M_{1,2}|$, is more stringent than that for the instability at the edge, $2J < |M_1 - M_2|$.

Next, we consider polarization of chiral modes. As we found above, the modes of both helicities, ψ_+ and ψ_- , propagate in the same direction. This gives rise to an interesting space-time picture that combines propagation with velocity v_g and precession about \mathbf{h}_0 . Indeed, a narrow wavepacket u_q centered at $q \approx q_0$ evolves as

$$\delta \mathbf{n}(r, t) = \sum_{q>0} \phi_q^+(r, t) \begin{pmatrix} 1 \\ i \end{pmatrix} + \sum_{q<0} \phi_q^-(r, t) \begin{pmatrix} 1 \\ -i \end{pmatrix} \quad (19)$$

$$\sim e^{-\lambda_{q_0}|y|} u(x - v_g t) \begin{pmatrix} \cos[\omega_0 t - q_0 x + \theta_0] \\ \sin[\omega_0 t - q_0 x + \theta_0] \end{pmatrix}.$$

Here, $\phi_q^{\pm}(r, t) = e^{-i\omega_{\pm}(q)t + iqx - \lambda_q|y|} u_q$. The quantity $u(x)$ is the Fourier transform of u_q , $\omega_0 = \omega_+(q_0)$, v_g is the group velocity $d\omega/dq$ at $q = q_0$, θ_0 is a free parameter. This describes spin precession and 1D propagation, as illustrated in Fig. 1 (c).

Lastly, we discuss the relation between the analysis above and the collective spin excitations in QH ferromagnets. The seminal prediction of skyrmions in QH ferromagnets by Sondhi et al.[47] relies on the notion of an excess charge induced on a chiral spin texture, $\delta\rho(r) = \frac{1}{c}\sigma_{xy}B(r)$, a value that follows from the topological pumping argument [48, 49] with σ_{xy} the Hall conductivity of a filled Landau level and B the quantity in Eq.(5). This gives a contribution to the energy

$$\delta E = \int d^2r V_g \delta\rho(r), \quad (20)$$

where V_g is the gate voltage. Since $B(r) = \frac{\phi_0}{4\pi} \mathbf{n} \cdot \partial_1 \mathbf{n} \times \partial_2 \mathbf{n}$, the quantity in Eq.(20) is identical in form to our $-MB$ interaction (the second term in Eq.(3)). Furthermore, it is straightforward to link the prefactor with the orbital magnetization of a fully filled Landau level

$$M = \frac{1}{c} V_g \sigma_{xy}. \quad (21)$$

This relation follows from the thermodynamic relation $dM/d\mu = dn/dB_{\text{ext}}$ and the Streda formula $dn/dB_{\text{ext}} = \frac{\sigma_{xy}}{ce}$. Having reproduced the $-MB$ interaction in the QH framework, we are led to conclude that the chiral spin waves derived above must also occur in QH ferromagnets. While a detailed analysis should be deferred to future work, we expect that these modes differ in two distinct ways from various chiral charge and spin edge modes that have been widely investigated in QH systems [50–58]. First, their dispersion at small k will be quadratic rather than linear. Second, rather than being tightly confined to the edge on a magnetic length scale, these modes will feature a wider profile extending far into the bulk. The weak confinement may suppress scattering by edge disorder and boost the lifetimes for these modes.

Last, we envision that extending the pulsed gate spectroscopy of Refs. [28, 29] to probe the gate-confined electron puddles can allow to launch the chiral spin waves and detect them in a manner analogous to the time-domain detection of QH edge magnetoplasmons [59–62]. Further, electron-spin resonance (ESR) measurements on such puddles by the technique recently used to probe ESR in graphene[63] can provide direct information of the chiral mode dispersion. Indeed, for a puddle of circumference L the mode dispersion in Eq.(18), will translate into sidebands of the ESR resonance with frequencies

$$\omega_n = \omega(q_n), \quad q_n = 2\pi n/L, \quad (22)$$

with integer n . Here $n = 0$ is the fundamental ESR frequency and $n = 1, 2, 3, \dots$ describes a family of chiral mode excitations. The $\omega = \omega_n$ resonances will occur over a continuous background due to the 2D spin-wave continuum, Eq.(11). As an example, we consider a disk of circumference $L = 10 \mu\text{m}$ for which the minimal wavenumber is

$q_1 = 2\pi/L$. Estimating the stiffness as the e-e interaction at the Fermi wavelength scale, $J \sim e^2/(\kappa\lambda_F)$, and plugging realistic parameter values, we find the sideband frequency detuning of $\omega_1 - \omega_0 \approx 50$ MHz. This value is greater than $1/T_1$ found in Refs.[28, 29] and lies in a convenient spectral range for microwave measurements. We also note that, as discussed above, spin dynamics in our system is accompanied by a geometric electric field given in Eq.(6). The oscillating electric polarization induced by this field can be used for a direct electrical detection of the chiral spin-wave dynamics.

Summing up, the chiral edge excitations are a unique manifestation of geometric interactions in a metallic spin-polarized Fermi sea with a Berry band curvature. Despite occurring in a non-topological setting they are protected from backscattering by their chiral character. Correlated-electron phases that host chiral edge modes allowing excitations to propagate along system boundaries in a one-way manner are of keen interest for fundamental physics and are expected to harbor interesting applications. We describe the requirements for such modes to exist and argue that the chiral behavior and associated exotic physics are generic and readily accessible in state-of-the-art systems.

This work originated from fruitful discussions with Eli Zeldov. We thank Herbert Fertig, Steven Girvin, Bertrand Halperin, Efrat Shimshoni, Shivaji Sondhi and Kun Yang for useful comments on the preliminary version of this paper. This research was supported by the Science and Technology Center for Integrated Quantum Materials, National Science Foundation Grant No. DMR1231319.

-
- [1] E. Y. Andrei and A. H. MacDonald, Graphene bilayers with a twist, *Nature materials* **19**, 1265 (2020).
 - [2] Y. Cao, V. Fatemi, A. Demir, S. Fang, S. L. Tomarken, J. Y. Luo, J. D. Sanchez-Yamagishi, K. Watanabe, T. Taniguchi, E. Kaxiras, and et al., Correlated insulator behaviour at half-filling in magic-angle graphene superlattices, *Nature* **556**, 80–84 (2018).
 - [3] Y. Cao, V. Fatemi, S. Fang, K. Watanabe, T. Taniguchi, E. Kaxiras, and P. Jarillo-Herrero, Unconventional superconductivity in magic-angle graphene superlattices, *Nature* **556**, 43–50 (2018).
 - [4] U. Zondiner, A. Rozen, D. Rodan-Legrain, Y. Cao, R. Queiroz, T. Taniguchi, K. Watanabe, Y. Oreg, F. von Oppen, A. Stern, E. Berg, P. Jarillo-Herrero, and S. Ilani, Cascade of phase transitions and dirac revivals in magic-angle graphene, *Nature* **582**, 203 (2020).
 - [5] D. Wong, K. P. Nuckolls, M. Oh, B. Lian, Y. Xie, S. Jeon, K. Watanabe, T. Taniguchi, B. A. Bernevig, and A. Yazdani, Cascade of electronic transitions in magic-angle twisted bilayer graphene, *Nature* **582**, 198 (2020).
 - [6] Y. Saito, F. Yang, J. Ge, X. Liu, T. Taniguchi, K. Watanabe, J. Li, E. Berg, and A. F. Young, Isospin pomeranchuk effect in twisted bilayer graphene, *Nature* **592**, 220 (2021).
 - [7] H. Zhou, L. Holleis, Y. Saito, L. Cohen, W. Huynh, C. L. Patterson, F. Yang, T. Taniguchi, K. Watanabe, and A. F. Young, Isospin magnetism and spin-polarized superconductivity in bernal bilayer graphene, *Science* **375**, 774 (2022).
 - [8] A. M. Seiler, F. R. Geisenhof, F. Winterer, K. Watanabe, T. Taniguchi, T. Xu, F. Zhang, and R. T. Weitz, Quantum cascade of new correlated phases in trigonally warped bilayer graphene, *arXiv preprint arXiv:2111.06413* (2021).
 - [9] S. C. de la Barrera, S. Aronson, Z. Zheng, K. Watanabe, T. Taniguchi, Q. Ma, P. Jarillo-Herrero, and R. Ashoori, Cascade of isospin phase transitions in bernal bilayer graphene at zero magnetic field, *arXiv preprint arXiv:2110.13907* (2021).
 - [10] H. Zhou, T. Xie, A. Ghazaryan, T. Holder, J. R. Ehrets, E. M. Spanton, T. Taniguchi, K. Watanabe, E. Berg, M. Serbyn, and A. F. Young, Half-and quarter-metals in rhombohedral trilayer graphene, *Nature* **598**, 429 (2021).
 - [11] H. Zhou, T. Xie, T. Taniguchi, K. Watanabe, and A. F. Young, Superconductivity in rhombohedral trilayer graphene, *Nature* **598**, 434 (2021).
 - [12] K. Ohgushi, S. Murakami, and N. Nagaosa, Spin anisotropy and quantum hall effect in the kagomé lattice: Chiral spin state based on a ferromagnet, *Physical Review B* **62**, R6065 (2000).
 - [13] T. Fujita, M. Jalil, S. Tan, and S. Murakami, Gauge fields in spintronics, *Journal of applied physics* **110**, 17 (2011).
 - [14] N. Nagaosa and Y. Tokura, Emergent electromagnetism in solids, *Physica Scripta* **2012**, 014020 (2012).
 - [15] K. Hamamoto, M. Ezawa, and N. Nagaosa, Quantized topological hall effect in skyrmion crystal, *Physical Review B* **92**, 115417 (2015).
 - [16] S. M. Girvin, Spin and isospin: exotic order in quantum hall ferromagnets, *Phys. Today* **53**, 39 (2000).
 - [17] K. Nomura and A. H. MacDonald, Quantum hall ferromagnetism in graphene, *Physical review letters* **96**, 256602 (2006).
 - [18] J. Alicea and M. P. Fisher, Graphene integer quantum hall effect in the ferromagnetic and paramagnetic regimes, *Physical Review B* **74**, 075422 (2006).
 - [19] K. Yang, S. D. Sarma, and A. MacDonald, Collective modes and skyrmion excitations in graphene s u (4) quantum hall ferromagnets, *Physical Review B* **74**, 075423 (2006).
 - [20] I. Spielman, J. Eisenstein, L. Pfeiffer, and K. West, Resonantly enhanced tunneling in a double layer quantum hall ferromagnet, *Physical review letters* **84**, 5808 (2000).
 - [21] J. Eisenstein, Exciton condensation in bilayer quantum hall systems, *Annu. Rev. Condens. Matter Phys.* **5**, 159 (2014).
 - [22] J. Eisenstein and A. MacDonald, Bose–einstein condensation of excitons in bilayer electron systems, *Nature* **432**, 691 (2004).
 - [23] J. Li, T. Taniguchi, K. Watanabe, J. Hone, and C. Dean, Excitonic superfluid phase in double bilayer graphene, *Nature Physics* **13**, 751 (2017).
 - [24] A. Finck, J. Eisenstein, L. Pfeiffer, and K. West, Quantum hall exciton condensation at full spin polarization, *Physical Review Letters* **104**, 016801 (2010).
 - [25] W. Han, K. McCreary, K. Pi, W. Wang, Y. Li, H. Wen, J. Chen, and R. Kawakami, Spin transport and relaxation in graphene, *Journal of Magnetism and Magnetic*

- Materials **324**, 369 (2012).
- [26] D. Kochan, M. Gmitra, and J. Fabian, Spin relaxation mechanism in graphene: resonant scattering by magnetic impurities, *Physical review letters* **112**, 116602 (2014).
 - [27] D. Kochan, S. Irmer, M. Gmitra, and J. Fabian, Resonant scattering by magnetic impurities as a model for spin relaxation in bilayer graphene, *Physical Review Letters* **115**, 196601 (2015).
 - [28] L. Banszerus, K. Hecker, S. Möller, E. Icking, K. Watanabe, T. Taniguchi, C. Volk, and C. Stampfer, Spin relaxation in a single-electron graphene quantum dot, *Nature Communications* **13**, 3637 (2022).
 - [29] L. M. Gächter, R. Garreis, J. D. Gerber, M. J. Ruckriegel, C. Tong, B. Kratochwil, F. K. de Vries, A. Kurzmänn, K. Watanabe, T. Taniguchi, T. Ihn, K. Ensslin, and W. W. Huang, Single-shot spin readout in graphene quantum dots, *PRX Quantum* **3**, 020343 (2022).
 - [30] See supplementary information, where we analyze the decay of the edge spin wave due to Landau damping, and the decay due to edge-to-bulk scattering enabled by the edge roughness. [url will be inserted by publisher].
 - [31] A. Mook, J. Henk, and I. Mertig, Edge states in topological magnon insulators, *Physical Review B* **90**, 024412 (2014).
 - [32] K. Mæland and A. Sudbø, Quantum topological phase transitions in skyrmion crystals, *arXiv preprint arXiv:2205.12965* (2022).
 - [33] S. A. Díaz, J. Klinovaja, and D. Loss, Topological magnons and edge states in antiferromagnetic skyrmion crystals, *Physical review letters* **122**, 187203 (2019).
 - [34] F. Garcia-Sanchez, P. Borys, A. Vansteenkiste, J.-V. Kim, and R. L. Stamps, Nonreciprocal spin-wave channeling along textures driven by the Dzyaloshinskii-Moriya interaction, *Physical Review B* **89**, 224408 (2014).
 - [35] P. A. McClarty, Topological magnons: A review, *Annual Review of Condensed Matter Physics* **13**, 171 (2022).
 - [36] R. Shindou, R. Matsumoto, S. Murakami, and J.-i. Ohe, Topological chiral magnonic edge mode in a magnonic crystal, *Physical Review B* **87**, 174427 (2013).
 - [37] R. Shindou, J.-i. Ohe, R. Matsumoto, S. Murakami, and E. Saitoh, Chiral spin-wave edge modes in dipolar magnetic thin films, *Physical Review B* **87**, 174402 (2013).
 - [38] J. C. Song and M. S. Rudner, Chiral plasmons without magnetic field, *Proceedings of the National Academy of Sciences* **113**, 4658 (2016).
 - [39] N. Nagaosa, *Quantum field theory in condensed matter physics* (1999).
 - [40] E. Fradkin, *Field theories of condensed matter physics* (2013).
 - [41] Z. Dong and L. Levitov, Chiral Stoner magnetism in Dirac bands, *arXiv preprint arXiv:2208.02051* (2022).
 - [42] G. Baskaran and P. W. Anderson, Gauge theory of high-temperature superconductors and strongly correlated Fermi systems, *Physical Review B* **37**, 580 (1988).
 - [43] P. Wiegmann, Superconductivity in strongly correlated electronic systems and confinement versus deconfinement phenomenon, *Physical review letters* **60**, 821 (1988).
 - [44] H. Schulz, Effective action for strongly correlated fermions from functional integrals, *Physical review letters* **65**, 2462 (1990).
 - [45] L. Ioffe, V. Kalmeyer, and P. Wiegmann, Hall coefficient of the doped Mott insulator: A signature of parity violation, *Physical Review B* **43**, 1219 (1991).
 - [46] C. Back, V. Cros, H. Ebert, K. Everschor-Sitte, A. Fert, M. Garst, T. Ma, S. Mankovsky, T. Monchesky, M. Mostovoy, et al., The 2020 skyrmionics roadmap, *Journal of Physics D: Applied Physics* **53**, 363001 (2020).
 - [47] S. L. Sondhi, A. Karlhede, S. Kivelson, and E. Rezayi, Skyrmions and the crossover from the integer to fractional quantum Hall effect at small Zeeman energies, *Physical Review B* **47**, 16419 (1993).
 - [48] D. Thouless, Quantization of particle transport, *Physical Review B* **27**, 6083 (1983).
 - [49] Q. Niu and D. Thouless, Quantised adiabatic charge transport in the presence of substrate disorder and many-body interaction, *Journal of Physics A: Mathematical and General* **17**, 2453 (1984).
 - [50] N. Balaban, U. Meirav, H. Shtrikman, and V. Umansky, Observation of the logarithmic dispersion of high-frequency edge excitations, *Physical Review B* **55**, R13397 (1997).
 - [51] V. Mazo, H. Fertig, and E. Shimshoni, Collective edge modes of a quantum Hall ferromagnet in graphene, *Physical Review B* **86**, 125404 (2012).
 - [52] P. Tikhonov, E. Shimshoni, H. Fertig, and G. Murthy, Emergence of helical edge conduction in graphene at the $\nu = 0$ quantum Hall state, *Physical Review B* **93**, 115137 (2016).
 - [53] S. Iordanski and A. Kasbuba, Excitations in a quantum Hall ferromagnet with strong Coulomb interaction, *Journal of Experimental and Theoretical Physics Letters* **75**, 348 (2002).
 - [54] A. Karlhede, K. Lejnell, and S. Sondhi, Dynamics of the compact, ferromagnetic $\nu = 1$ edge, *Physical Review B* **60**, 15948 (1999).
 - [55] Y. Zhang and K. Yang, Edge spin excitations and reconstructions of integer quantum Hall liquids, *Physical Review B* **87**, 125140 (2013).
 - [56] M. Kharitonov, S. Juergens, and B. Trauzettel, Interplay of topology and interactions in quantum Hall topological insulators: U(1) symmetry, tunable Luttinger liquid, and interaction-induced phase transitions, *Physical Review B* **94**, 035146 (2016).
 - [57] A. Saha, S. J. De, S. Rao, Y. Gefen, and G. Murthy, Emergence of spin-active channels at a quantum Hall interface, *Physical Review B* **103**, L081401 (2021).
 - [58] U. Khanna, M. Goldstein, and Y. Gefen, Emergence of neutral modes in Laughlin-like fractional quantum Hall phases, *Physical Review Letters* **129**, 146801 (2022).
 - [59] R. Ashoori, H. Stormer, L. Pfeiffer, K. Baldwin, and K. West, Edge magnetoplasmons in the time domain, *Physical Review B* **45**, 3894 (1992).
 - [60] N. Zhitenev, R. Haug, K. v. Klitzing, and K. Eberl, Time-resolved measurements of transport in edge channels, *Physical review letters* **71**, 2292 (1993).
 - [61] G. Ernst, R. Haug, J. Kuhl, K. von Klitzing, and K. Eberl, Acoustic edge modes of the degenerate two-dimensional electron gas studied by time-resolved magnetotransport measurements, *Physical review letters* **77**, 4245 (1996).
 - [62] N. Kumada, H. Kamata, and T. Fujisawa, Edge magnetoplasmon transport in gated and ungated quantum Hall systems, *Physical Review B* **84**, 045314 (2011).
 - [63] J. Sichau, M. Prada, T. Anlauf, T. Lyon, B. Bosnjak, L. Tiemann, and R. Blick, Resonance microwave measurements of an intrinsic spin-orbit coupling gap in graphene: A possible indication of a topological state, *Physical Review Letters* **122**, 046403 (2019).

SUPPLEMENTARY INFORMATION

Here, we consider intrinsic mechanisms of the edge spin wave damping. We first discuss the Landau damping due to the 2D particle-hole continuum ignoring edge roughness, and then consider the decay pathway that is enabled by the edge roughness. We argue that both mechanisms give damping that becomes negligible at long wavelengths and low frequencies.

The particle-hole continuum in spin-polarized metals, that can potentially lead to Landau damping of collective spin excitations, consists of two distinct parts: the spin-zero continuum and the spin-one continuum. The spin-zero particle-hole continuum spans wavenumbers $0 < k < 2k_F$ and extends in frequency down to $\omega = 0$. Spin waves cannot simply decay into these excitations owing to the spin U(1) symmetry that ensures spin conservation. Therefore, these excitations do not impact the spin-wave lifetimes on a tree level. Scattering involving spin-zero continuum can only take place through higher-order processes in which a spin wave is scattered by a spin-zero excitation or emits it without decaying. However, such processes are suppressed by the phase space volume for the final states.

Another 2D particle-hole continuum nominally available for decay, which is not blocked by the spin conservation, is the spin-one continuum, in which an electron is excited from the spin-majority band to the spin-minority band. However, the spin-one excitations are fully gapped at small momenta [see Fig.2 (a)] and, as a result, this scattering pathway is absent for long-wavelength (low-frequency) spin waves. Moreover, for the fully spin-polarized phase, the spin-one excitation is fully gapped at all momenta, which fully protects the long-wavelength spin waves from the edge-to-bulk scattering.

Next, we study the scattering from the spin wave edge mode to bulk spin waves by edge disorder, and show that the lifetime is ultra-long for long-wavelength edge modes. As a simple model, we consider a step in magnetization with a wiggly boundary, illustrated in Fig. 2 (b). We will describe spin waves by a problem linearized in a weak perturbation about the uniform state, as implemented in the main text [see Eq.(7) therein]. Using the right and left helicity representation [see Eq.(14) of the main text] and, without loss of generality, focusing on the ψ_+ mode, we arrive at an effective action

$$A = \int dt d^2r \bar{\psi}_+ (i\partial_t - H) \psi_+, \quad (23)$$

where $H = h_0 - \frac{J}{2}(\partial_x^2 + \partial_y^2) + \epsilon_{jj'}\partial_j M(r)\partial_{j'}$, and $M(r)$ describes two domains with magnetization M_1 and M_2 [Fig.2 (b)]. The magnetization gradient $\partial_j M(r)$ is a delta function centered at the wiggly domain boundary. For conciseness, we suppressed factors such as n_s , S_0 , etc.

A convenient way to carry out the analysis is to employ a coordinate change that transforms a modulated

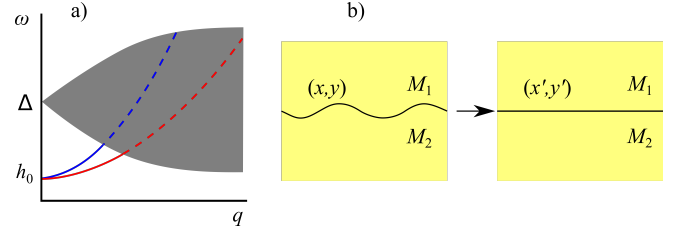


FIG. 2. (a) Collective spin excitations in the bulk (blue line) and at the edge (red line) superimposed with the spin-one particle-hole continuum (gray region). Below the Stoner gap $\Delta = Un_s$ the collective modes are decoupled from the continuum and are therefore discrete. Upon entering the continuum they become Landau-damped (dashed lines). The spin-zero particle-hole continuum with wavenumbers $0 < k < 2k_F$ and frequencies extending down to $\omega = 0$ is not shown. This continuum is irrelevant for the damping of spin waves since one-excitation processes are blocked by U(1) spin conservation. (b) A wiggly step in magnetization $M(r)$ representing a rough edge. By a conformal mapping, Eq.(24), the problem with a wiggly edge is mapped onto the one with a straight edge and a fluctuating metric localized near the edge, Eq.(25). The edge-to-bulk scattering gives rise to a finite lifetime of the edge mode, $\tau = 1/\gamma$, where γ is given in Eq.(26).

boundary into a straight one. This can be done by a conformal mapping defined by an analytic function in the halfplane $y > 0$ and an anti-analytic function in the halfplane $y < 0$ with values matching at $y = 0$. The most general function of this type is of the form

$$z' = x' + iy' = z + \sum_k g_k e^{ikx - |k||y|}. \quad (24)$$

Under such conformal mapping the Schroedinger operator in Eq.(23) preserves its form up to a change in coefficients, allowing to describe a wiggly edge as a straight edge with a perturbation in the metric localized in its vicinity. The simple transformation rule is a consequence of the conformal invariance of the 2D Laplacian and the chiral density terms in our Hamiltonian, Eq.(3) in the main text. Indeed, denoting the Jacobian of the mapping in Eq.(24) as $D(r) = (\partial x', \partial y')/(\partial x, \partial y)$, we find that under the conformal mapping the terms $i\partial_t - h_0$ in Eq.(23) are multiplied by D^{-1} whereas other terms remain unchanged.

The lifetime can now be calculated from the selfenergy for the Greens function

$$G = \frac{1}{\omega - H} = \frac{1}{\frac{\omega - h_0}{D(r)} + J(\partial_x^2 + \partial_y^2) - im\delta(y)\partial_x}$$

Expanding the Jacobian in powers of the modulation amplitude g_k gives $D^{-1}(r) = 1 + \delta p(r)$ where $\delta p(r) = \sum_k k g_k e^{ikx - |k||y|} + \text{c.c.} + O(g_k^2)$. We can now rewrite the Greens function in terms of the Hamiltonian for the straight edge, $H_0 = h_0 - J(\partial_x^2 + \partial_y^2) + im\delta(y)\partial_x$, and the

perturbation $\delta p(r)$ localized near the edge:

$$G = \frac{1}{\omega - H_0 + (\omega - h_0)\delta p(r)}. \quad (25)$$

This expression is exact and can therefore be used to obtain the lifetime of the chiral edge mode in a closed form. Starting with a normalized wavefunction for the chiral mode derived above, $|\psi_+^0\rangle = e^{iqx}e^{-\lambda_q|y|}\lambda_q^{1/2}$, and calculating the lifetime from the selfenergy of G found at second order in $\delta p(r)$ we find the decay rate

$$\gamma = 2\pi \sum_{\mathbf{Q}} \text{Im}G_0(\omega, \mathbf{Q}) |\langle e^{i\mathbf{Q}r} | (\omega - h_0)\delta p(r) | \psi_+^0 \rangle|^2$$

where $G_0 = \frac{1}{\omega - H_0 + i0}$ and \mathbf{Q} is the bulk magnon momentum. For a simple order of magnitude estimate

it will be sufficient to approximate the spectral function $\text{Im}G_0(\omega, \mathbf{Q})$ as that of the bulk magnon continuum, $\text{Im}G_0(\omega, \mathbf{Q}) = \pi\delta(\omega - J\mathbf{Q}^2)$. Estimating this expression we find the decay rate that scales as

$$\gamma \sim \lambda_q(\omega - h_0)^2 \quad (26)$$

At small q these quantities scale as $\lambda_q \sim |q|$, $\omega - h_0 \sim q^2$ yielding the decay rate that vanishes in the long-wavelength limit as $\gamma \sim q^5$. The long lifetime arises as a combination of two effects. First, because of the Larmor theorem, in the small q limit the mode frequency for both bulk and edge is pinned to h_0 regardless of the presence of an edge disorder. Second, because at small q the edge mode has a large penetration length into the bulk, $1/\lambda$. As a result, the mode weakly overlaps with the edge roughness, which suppresses the edge-to-bulk scattering.